



HAL
open science

Molecular dynamics study of confined water in the periclase-brucite system under conditions of reaction-induced fracturing

Marthe Guren, Henrik Sveinsson, Anders Hafreager, Bjørn Jamtveit, Anders Malthe-Sørenssen, François Renard

► To cite this version:

Marthe Guren, Henrik Sveinsson, Anders Hafreager, Bjørn Jamtveit, Anders Malthe-Sørenssen, et al.. Molecular dynamics study of confined water in the periclase-brucite system under conditions of reaction-induced fracturing. *Geochimica et Cosmochimica Acta*, 2021, 294, pp.13-27. 10.1016/j.gca.2020.11.016 . insu-04095633

HAL Id: insu-04095633

<https://insu.hal.science/insu-04095633>

Submitted on 12 May 2023

HAL is a multi-disciplinary open access archive for the deposit and dissemination of scientific research documents, whether they are published or not. The documents may come from teaching and research institutions in France or abroad, or from public or private research centers.

L'archive ouverte pluridisciplinaire **HAL**, est destinée au dépôt et à la diffusion de documents scientifiques de niveau recherche, publiés ou non, émanant des établissements d'enseignement et de recherche français ou étrangers, des laboratoires publics ou privés.



Distributed under a Creative Commons Attribution 4.0 International License



Molecular dynamics study of confined water in the periclase-brucite system under conditions of reaction-induced fracturing

Marthe G. Guren^{a,*}, Henrik A. Sveinsson^a, Anders Hafreager^a, Bjørn Jamtveit^a,
Anders Malthe-Sørensen^a, François Renard^{a,b}

^a *The Njord Centre, Departments of Geoscience and Physics, University of Oslo, Norway*

^b *University Grenoble Alpes, University Savoie Mont Blanc, CNRS, IRD IFSTTAR, ISTERre, 38000 Grenoble, France*

Received 7 July 2020; accepted in revised form 16 November 2020; available online 24 November 2020

Abstract

The volume-increase associated with hydration reactions in rocks may lead to reaction-induced fracturing, but requires a stable water film to be present at reactive grain boundaries even when subject to compressive stress. Hydration of periclase to brucite is associated with a solid volume increase of ca. 110%. Recent experiments on the periclase-brucite system observed that when the effective mean stress exceeds 30 MPa, the reaction rate slows down dramatically. We hypothesize that for the brucite forming reaction to progress, the fluid film between grains must remain stable. If the applied pressure becomes larger than the hydration force, the fluid film will collapse and be squeezed out of the grain contacts. To quantify this effect, we study the behavior of a water film confined between periclase or brucite surfaces subject to compressive stress, by performing molecular dynamics simulations. The simulations are carried out using the ClayFF force field and the single point charge (SPC) water model in the molecular dynamics simulations program LAMMPS. The setup consists of two interfaces of either periclase or brucite surrounded by water. Our simulations show that when the pressure reaches a few tens of MPa, the water film collapses and reduces the water film to one or two water layers, while the self-diffusion coefficient of water molecules by a factor of eight. A water film thickness below two water layers is thinner than the size of the hydration shell around Mg^{2+} -ions, which will limit ion-transport. The observed collapse of the water film to a single layer at a normal pressure of 25–30 MPa might explain the observed slow-down of reaction-induced fracturing in the periclase-brucite system.

© 2020 The Author(s). Published by Elsevier Ltd. This is an open access article under the CC BY license (<http://creativecommons.org/licenses/by/4.0/>).

Keywords: Brucite; Periclase; Hydration force; Confined water; Reaction-induced fracturing

1. INTRODUCTION

Interactions between aqueous solutions and rocks occur in a wide range of environments, from weathering near the Earth's surface to metamorphic reactions in the lower crust. These interactions control the transformations of rocks from one type to another (Jamtveit and Hammer, 2012;

Harlov and Austrheim, 2012; Putnis, 2014). Such transformations depend on nanoscale mechanisms controlled by fluid-rock interactions and porosity evolution (Røyne and Jamtveit, 2015). Fluids control the transport of chemical components to and from the grain surfaces where the reactions occur and the supply rate of these components affects the overall rock transformation rate, for example during serpentinization of peridotites (Martin and Fyfe, 1970; Putnis, 2002; Zhang et al., 2019). Reactions at grain contacts in rocks require the presence of porosity, that provides

* Corresponding author.

E-mail address: m.g.guren@geo.uio.no (M.G. Guren).

fluid pathways, and a fluid film confined along grain boundaries. When this fluid film collapses to two or one water layers, water transport rates decrease, slowing down the reaction rate, as proposed in the context of rock deformation by pressure solution creep (Renard and Ortoleva, 1997; Dysthe et al., 2002). In the present study, we explore the behavior of water confined between periclase or brucite surfaces under conditions where reaction-induced fracturing occurs.

Reaction-induced fracturing is a process whereby the hydration reaction of minerals produces a volume increase leading to the build-up of a force of crystallization and rock fracturing (Martin and Fyfe, 1970; Scherer, 2004). Examples are the hydration of periclase to brucite that occurs with a 110 % solid volume increase and a 45 % weight increase (Kuleci et al., 2016; Zheng et al., 2018), the hydration of calcium oxide to portlandite with a 50 % volume increase (Kelemen et al., 2011), and reactions leading to rock weathering (Røyne et al., 2008). Reaction-induced fracturing may also occur in geo-engineering applications, for example in slowly expanding cements used to prevent leakage in borehole casings (Wolterbeek et al., 2018).

In the Earth's crust, one of the most important reaction-induced fracturing processes is serpentinization (e.g. Martin and Fyfe, 1970) where the hydration of olivine grains can lead to 50 % volume increase (Malvoisin et al., 2017), creating a fracture network in the host rock and enabling fluid circulation and creation of new reactive surface areas. These fractures have been studied extensively in both experiments and numerical models (e.g. Jamtveit et al., 2009; Kelemen and Hirth, 2012; Plümper et al., 2012; Zheng et al., 2018; Zhang et al., 2019), and it has been suggested that the rate of serpentinization is controlled by the rate of water supply to the reaction surface (Martin and Fyfe, 1970). Observations imply that, as the olivine grains are fragmented, the hydration reaction is accelerated because it provides fluid pathways to newly exposed reactive surfaces (Iyer et al., 2008; Zhang et al., 2019).

During mineral hydration and volume increase, a pressure, called the force of crystallization, is produced. This pressure, exerted when a crystal grows from a supersaturated fluid, corresponds to the maximum force this crystal can exert on a solid surface before the reaction stops (Weyl, 1959). The force of crystallization of a hydration reaction can be calculated from thermodynamic data of both the host and forming crystals (Weyl 1959; Eq. 13 in Wolterbeek et al., 2018):

$$\sigma_{\text{force of crystallization}} = \frac{\Delta_f G_i^{P,T} + \Delta_f G_{H_2O}^{P,T} - \Delta_f G_j^{P,T}}{V_{m,j}^{P,T} - V_{m,i}^{P,T}} \quad (1)$$

where the subscripts i and j correspond to the host mineral and forming mineral, $\Delta_f G^{P,T}$ is the Gibbs free energy and $V_m^{P,T}$ is the molar volume, both at the given pressure and temperature conditions. This force has been measured in a series of experiments where crystals were grown from a supersaturated solution (e.g. Becker and Day, 1916; Correns, 1949; Ostapenko, 1976; Scherer, 2004). Recent studies on the hydration of minerals indicate that the experimental and theoretical values of the force of crystallization

may differ by one or two orders of magnitude (Hövelmann et al. (2012); Kelemen and Hirth, 2012; Kuleci et al., 2016; Wolterbeek et al., 2018; Zheng et al., 2018). These large differences could come from a different thermodynamic limit than that given by equation (1) or from a kinetics effect where the reaction would slow down or stop at a pressure much lower than the thermodynamic limit. Experiments have shown that the kinetics of hydration of calcium oxide to portlandite slows down above 135 MPa, compared to the thermodynamic limit of 3.4 GPa (Wolterbeek et al., 2018). Zheng et al. (2018) observed a similar trend for the hydration of periclase to brucite, with a slowdown of the kinetics of transformation above 30 MPa, compared to a calculated thermodynamic limit of 1.9 GPa.

Our study builds on the experimental results of Zheng et al. (2018) who quantified the reaction-induced fracturing process when periclase (MgO) is hydrated into brucite (Mg(OH)₂) at temperatures in the range 453–473 K, through the reaction $\text{MgO} + \text{H}_2\text{O} \rightarrow \text{Mg(OH)}_2$. This reaction leads to the build-up of a force of crystallization and fracturing of the solid. Zheng et al. (2018) characterized the processes by *in situ* imaging using 4D synchrotron X-ray microtomography with micrometer spatial sampling. They showed that when the effective mean stress applied on the periclase core exceeds ca. 30 MPa, the rate of reaction-induced fracturing slowed down dramatically (Fig. 1a). They interpreted this effect to arise from the removal of water from the grain-grain interfaces. Kuleci et al. (2016) proposed that three kinetic parameters may control the overall rate of the reaction-induced process in the periclase-brucite system: the dissolution rate of periclase; the diffusion rate of ions from periclase to brucite; and the growth rate of brucite. These parameters may control why the brucite-forming reaction slows down under certain conditions of pressure and temperature (Kuleci et al., 2016; Zheng et al., 2018). However, a physical understanding of Zheng et al. (2018) interpretation is lacking and the effect of pressure on the proposed parameters (Kuleci et al., 2016) remains to be characterized.

To increase our understanding of why theoretical and experimental approaches gives such different force of crystallization values, we explore the hypothesis proposed by Zheng et al. (2018) and Kuleci et al. (2016). We study if the water is removed from the grain-grain interface when the normal stress is increasing, and how this affects the diffusion rate of Mg²⁺ ions from periclase to brucite along the grain contacts. The results are obtained from several series of molecular dynamic simulations under conditions relevant for reaction-induced fracturing. Our goal is to characterize the transport properties and hydration force in a water film confined along the interface between two grains.

The grains in the simulations consist of brucite or periclase. Experiments on the hydroxylation process of periclase (e.g. Refson et al., 1995; Oviedo et al., 1998; Lee et al., 2003; Jug et al., 2007) have demonstrated that the periclase (1 0 0) surface restructures into the (1 1 1) crystallographic face when it hydroxylates. This hydroxylated surface shows a similar organization of the atoms as a brucite (0 0 1) surface (Fig. 1b). In periclase (1 1 1) and brucite (0 0 1), the Mg and O atoms are organized in alternating

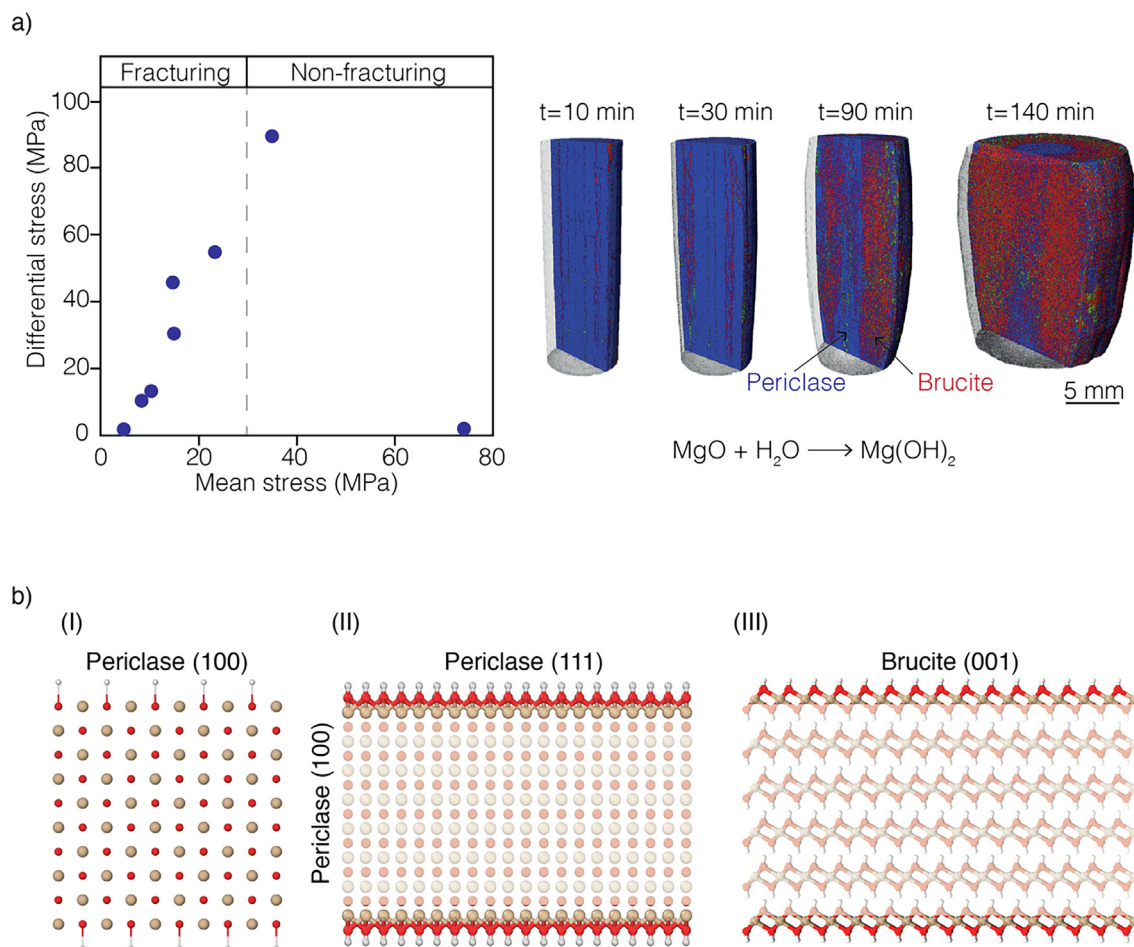


Fig. 1. (a) Experiments of reaction-induced fracturing in the periclase-brucite system performed by Zheng et al. (2018). The blue circles in the diagram represent experimental conditions and the dashed line separates two domains: below ~ 30 MPa mean effective stress, reaction-induced fracturing of periclase was observed, and above 30 MPa this reaction was not observed during the duration of these experiments. The four cylinders show an experiment performed below 30 MPa mean stress where the transformation from periclase (blue) to brucite (red) with time occurred with a volume increase of 110 % and reaction-induced fracturing of the initial periclase core. (b) Molecular-scale representation of the hydrated surfaces of periclase and brucite. Magnesium atoms are beige, oxygen atoms are red and hydrogen atoms are white. (I) A theoretical hydroxylated periclase (1 0 0) surface. (II) A hydrated periclase (1 1 1) surface, where the top and bottom layers are almost identical to brucite. (III) A brucite (0 0 1) surface. (For interpretation of the references to colour in this figure legend, the reader is referred to the web version of this article.)

planes (Wogelius et al., 1995). We assume that a non-hydroxylated (1 0 0) periclase surface will hydroxylate when it comes in contact with water, creating the (1 1 1) face. The ClayFF force field and later improvements (Cygan et al., 2004; Zeitler et al., 2014; Pouvreaux et al., 2017) have been developed for the brucite (0 0 1) face and these values are not necessarily transferrable to the periclase (1 1 1) face. We build on these findings and consider a water film confined between two brucite (0 0 1) surfaces or two non-hydroxylated periclase (1 0 0) surfaces and identify the behavior and properties of the water film under conditions relevant for reaction-induced fracturing. In particular, we determine what stress is necessary to squeeze out layers of the water film from the grain contacts, and how the removal of water layers influences the transport properties of the water film.

2. COMPUTATIONAL METHODS

To study the behavior and properties of a confined water film, we perform four series of simulations; labelled *Brucite-squeeze*, *Periclase-squeeze*, *Brucite-transport* and *Periclase-transport* (Table 1). The first name refers to the mineral system, and the second name represents the procedure (*squeeze* out the water film or *transport* properties of a confined water film). Each setup consists of one or two mineral blocks surrounded by water molecules (Figs. 2 and 3a). The studied minerals are brucite ($\text{Mg}(\text{OH})_2$) and periclase (MgO).

The transport properties of a water film confined between mineral surfaces are characterized by two parameters: the water film thickness and the self-diffusion coefficient of water molecules in this film (Renard and

Table 1
Overview of the molecular dynamics simulations conditions.

Simulation type	Slab [unit cells]	Pressure [MPa]	Temperature [K]
<i>Brucite-squeeze</i>	10 × 10 × 7	10–100	300, 360, 432, 520
	10 × 20 × 7	53	300, 520
	20 × 10 × 7	53	300, 520
	40 × 40 × 7	53	300, 520
<i>Periclase-squeeze</i>	7 × 13 × 7	10–100	300, 360, 432, 520
<i>Brucite-transport</i>	6 × 6 × 4	10–100	300, 360, 432, 520
<i>Periclase-transport</i>	5 × 5 × 5	10–100	300, 360, 432, 520

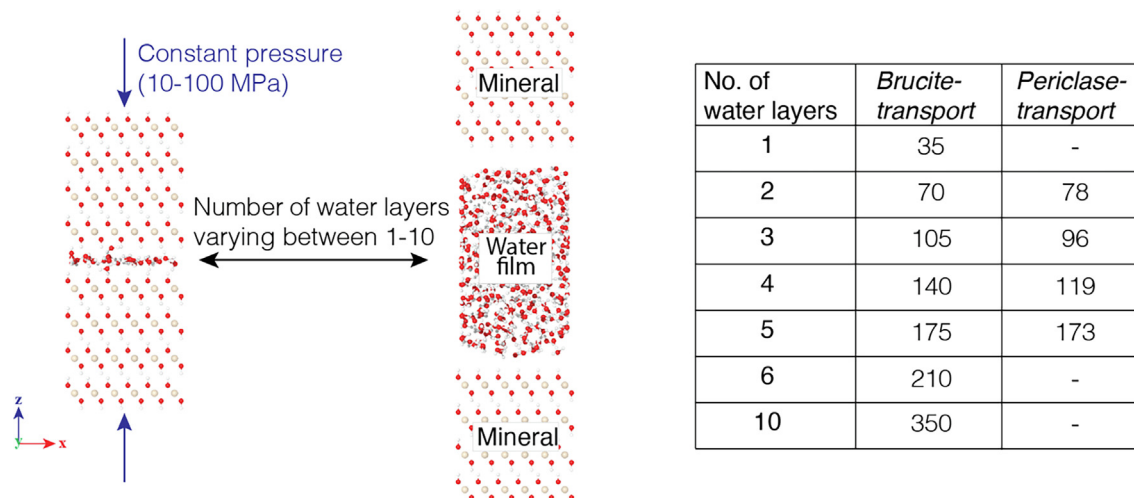


Fig. 2. Molecular dynamics simulation setups for the *Brucite-transport* and *Periclase-transport*. The setup consists of two mineral slabs with a water film confined between them. Conditions are periodic in the three directions. The water film thickness is varied between 1 and 10 layers and the number of water molecules in each layer is given in the table. The thickness of the water film is kept constant through each simulation, independent on pressure and temperature conditions. The mineral slab is periodic in the x- and y-directions. A gap between the mineral and water film is added for clarity. During the simulations, the dimensions of the 3D simulation domain vary with time.

Ortoleva, 1997; Dysthe et al., 2002). To address these two parameters, we use two different methods. The first method (*Brucite-transport* and *Periclase-transport*, Section 3.1, Fig. 2) is used to describe the self-diffusion coefficient of a confined water film. The second method (*Brucite-squeeze* and *Periclase-squeeze*, Section 3.2, Fig. 3) is used to study the change of the thickness of a water film with time when two solids are pushed towards each other. An alternative numerical setup to calculate the effect of pressure on water film thickness is presented in the Appendix (Texts A1, A2 and Fig. A1, A2).

In molecular dynamics simulations, we select a particular thermodynamic ensemble for the simulation. Depending on which ensemble is chosen, three thermodynamic parameters (e.g. temperature, pressure and number of atoms or energy, volume and number of atoms) will be held fixed, while the other parameters are calculated by performing various measurements on the system (Allen and Tildesley, 1987). In the present study, we apply a mechanical load on a solid surrounded by water by letting the simulation domain change with time in x-, y- and z-directions separately to achieve a particular mechanical stress in each coordinate direction (Fig. 3a). This lets us model a quasi-2D pore throat, representing a grain boundary, coupled

to a large pore space. The mechanical stress and the temperature are applied by a Nosé-Hoover barostat and thermostat (Shinoda et al., 2004).

We run the simulations with the open source program LAMMPS (Plimpton, 1995), together with the ClayFF force field for the minerals (Cygan et al., 2004). To simulate water, the single point charge (SPC) water model is used because it is compatible with the ClayFF force field (Berendsen et al., 1987; Cygan et al., 2004). Table 2 provides the force field parameters for periclase, brucite and water. The ClayFF force field was developed for clays and hydrated mineral in aqueous solutions, and reproduces bulk properties of clays, including infinite hydroxylated surfaces (Cygan et al., 2004). However, one limitation is that hydroxyl groups on edges and corners of finite size nanoparticles may detach unrealistically and migrate away from the mineral structure (Zeitler et al., 2014; Pouvreau et al., 2017). Zeitler et al. (2014) developed a non-bonded three-body angle term for Mg-O-H in brucite, later improved by Pouvreau et al. (2017), to limit this detachment. We observe that the number of hydroxyl groups that detach in simulations with and without the angle term is quite similar. However, with an angle term, the simulation will stop if hydroxyl-groups detach and move away from

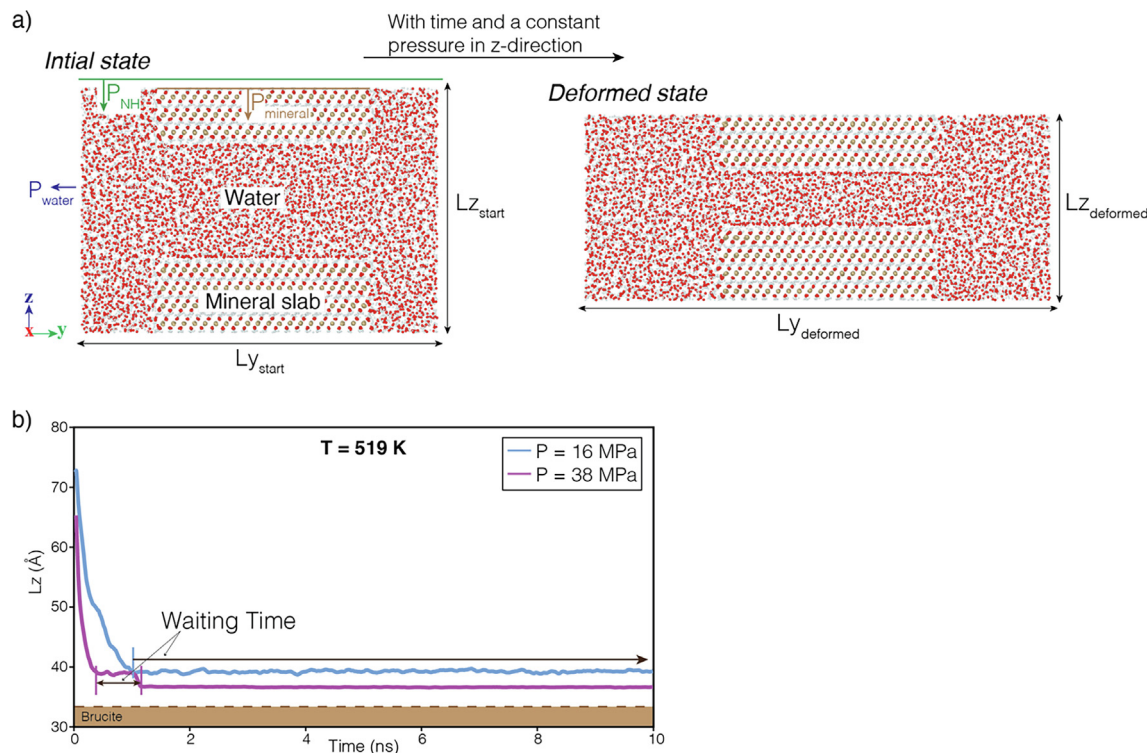


Fig. 3. (a) Molecular dynamics simulation setup for the *Brucite-squeeze* and *Periclase-squeeze* systems. The setup consists of one mineral slab surrounded by water in a three-dimensional domain with periodic boundary conditions. The mineral slab is continuous and periodic in the x-direction (pointing out of the paper plane) and surrounded by water in the y- and z-directions. A Nosé-Hoover barostat (P_{NH}) is applied in the z-direction of the simulation domain. With time, this pressure condition causes the simulation domain to deform ($LZ_{start} > LZ_{deformed}$ and $LY_{start} < LY_{deformed}$), slowly thinning the water films near the top and bottom surfaces of the brucite slab. (b) An example of two results from the *Brucite-squeeze* system showing the thickness (Lz) of the simulation domain in the z-direction as a function of time. This figure illustrates how we measure the waiting time. The waiting time is the time it takes for the water film to stabilize at one water layer between brucite grains and two water layers between periclase grains, within 10 ns time limit.

Table 2

Bonded and non-bonded parameters for the ClayFF force field. ¹Values from Zeidler et al. (2014). ²Values from Cygan et al. (2004).

Non-bonded parameters

Species	Charge (e) ¹	D_0 (kcal/mol) ¹	r (Å) ¹
H _{H2O}	0.41	0	0
O _{H2O}	-0.82	1.554	3.16684492
Mg _{MgO}	1.36	$9.030 \cdot 10^{-7}$	4.69188948
O _{MgO}	-1.36	0.1554	3.16684492
Mg _{Mg(OH)2}	1.05	$9.030 \cdot 10^{-7}$	4.69188948
O _{OH}	-0.95	0.1554	3.16684492
H _{OH}	0.425	0	0

Bonded parameters

Bond stretch (H_{H2O}-O_{H2O})

k_1 (kcal/mol Å ²) ²	Rigid
r_0 (Å) ²	1.0

Angle bend (H_{H2O}-O_{H2O}-H_{H2O})

k_1 (kcal/mol rad ²) ²	Rigid
angle (degrees) ²	109.47

the solid. Therefore, we run our simulations without the angle term, and ignore the detachment of hydroxyl groups.

We performed all simulations in the pressure range 10–100 MPa and temperature range 300–520 K, relevant for thermodynamic conditions in the Earth's upper crust. To

confirm that the force field parameters can be used at these conditions, we studied the evolution of the lattice parameters of brucite at these pressure and temperature ranges and compared with experimental values (Catti et al., 1995; Duffy et al., 1995; Nagai et al., 2000; Fukui et al.,

2003). The results of these simulations can be found in the Appendix (Text A3, Fig. A3) and show that the ClayFF force field can be used at the pressure and temperature conditions used in the present study. The conditions for the different simulations are given in Table 1.

2.1. Water transport and structural properties

The *Brucite-transport* and *Periclase-transport* simulations were performed to study the transport and structural properties of confined water films. The setup consists of two slabs of the same mineral, either periclase or brucite, with a water film confined between them (Fig. 2). These simulations were conducted in the NPT ensemble, where the number of atoms, the pressure and the temperature are held fixed. We used seven different water film thicknesses, varying in the range 1–10 water layers (Fig. 2). To study the structural properties of a confined water film between mineral surfaces, we calculated atomic density profiles for hydrogen and oxygen atoms between brucite surfaces in the *Brucite-transport* simulations, using a similar setup as in Wang et al. (2004). The self-diffusion coefficient of water molecules is calculated with two metrics. First, it is calculated as the average of the mean square displacement of water molecules over ten simulations where each run was executed for a duration of 10 ps with a timestep of 1 fs. Second, we used the velocity autocorrelation function and the simulation duration was decreased to 1 ps and sampled 100 times with a timestep of 1 fs. The velocity autocorrelation function (Fig. A4) was used to verify that the results are identical with both methods. The self-diffusion coefficients given in the results and discussions are measured with the mean square displacement. To estimate the activation energy, the diffusion constant is calculated at different temperatures and then an Arrhenius plot based on the equation $D = D_0 \times \exp(-E_a/R(T-T_0))$ is made, where D is the self-diffusion coefficient at temperature T , D_0 is the self-diffusion coefficient at $T_0 = 300$ K, E_a is the activation energy, and R is the gas constant. The activation energy of self-diffusion of water is calculated for all the water film thicknesses.

2.2. Setup to squeeze out a confined water film

For the *Brucite-squeeze* and *Periclase-squeeze* simulations, we placed a slab of either brucite or periclase in the middle of the simulation domain, and the slab was surrounded by water (Fig. 3a). For brucite, we used three different sizes of the slab (Table 1), where the larger systems are used to characterize the effect of domain size on the removal of water from the interface. For periclase, we used one size of the slab which was chosen such that the surface area was the same as for the smallest brucite slab. The slab spans the whole simulation domain in the x-direction, but leaves room for water in the y- and z-directions. Conditions are periodic in the three directions. The simulation domain contains an initial extra space of 4.1 nm in the y-direction and 3.4 nm in the z-direction, both spaces being filled with water (Fig. 3a). The simulations are run with a barostat set in the z-direction of the simulation domain. With time, the domain dimensions vary (Fig. 3a) as the domain is com-

pressed in the z-direction. At the same time, the domain extends in the y-direction to accommodate the water removed from the brucite interface, such that the water density in the entire system is conserved. We update the pressure on the domain walls (P_{NH}) every 10 ps to keep the pressure acting on the mineral surface (P_{mineral}) constant as the domain dimensions changes, following equation (2):

$$P_{NH} = \frac{P_{\text{mineral}} \cdot A_{\text{mineral}} + P_{\text{water}} \cdot (A_{\text{box}} - A_{\text{mineral}})}{A_{\text{box}}} \quad (2)$$

where P_{mineral} is the pressure acting on the mineral slabs (Fig. 3), P_{water} is the water pressure on the boundaries of the simulation domain. P_{water} is set to be constant and equal to 10 MPa, while P_{mineral} is kept constant by adjusting P_{NH} with time. A_{mineral} and A_{box} are the surface areas of the brucite slab and simulation domain, respectively, in the x- and y-directions.

The simulations are run for up to 10 ns. We measure the time it takes for the water film to stabilize at one water layer between brucite grains and two water layers between periclase grains, within 10 ns time limit. The last layer(s) of water are weakly bonded to the surfaces and will therefore stay trapped between the mineral surfaces. The waiting time to reach one or two water layers is measured in a series of simulations in the pressure range 15–40 MPa and 519 K.

2.3. Computational details

The mineral structures of periclase and brucite, with space groups Fm3m and P3m1 are constructed from published unit cells (Zigan and Rothbauer, 1967; Sasaki et al., 1979) using the Atomic Simulation Environment (ASE) software (Larsen et al., 2017). The water is simulated with the single point charge (SPC) model (Berendsen et al., 1987). In the simulation domain, the water has an initial density of 1000 kg/m³. To pack the water, randomly and without overlap, we use the software package packmol (Martinez and Martinez, 2003), and set the tolerance distance to 2.0 Å, which is the minimum distance between a mineral structure and water molecules. All simulations are run using periodic boundary conditions in the three directions of space. The ClayFF potential has a 12–6 Lennard-Jones potential. We set the cut-off distance to be 8.0 Å and set the long-range Coulombic interactions, calculated using particle–particle particle-mesh (pppm), with a relative precision of 10⁻⁴ (dimensionless). Harmonic bond stretching and angle bending between bonded atoms are optional. We enforce rigid bonds and angles of the water molecules and in hydroxyl groups of brucite using the SHAKE algorithm (Ryckaert et al., 1977). This allows for a time step of 1 fs during simulations.

3. RESULTS

3.1. Self-diffusion coefficient and density profiles in the confined water films

The atomic density profiles of oxygen (Fig. 4a) and hydrogen (Fig. A5) atoms in a direction perpendicular to

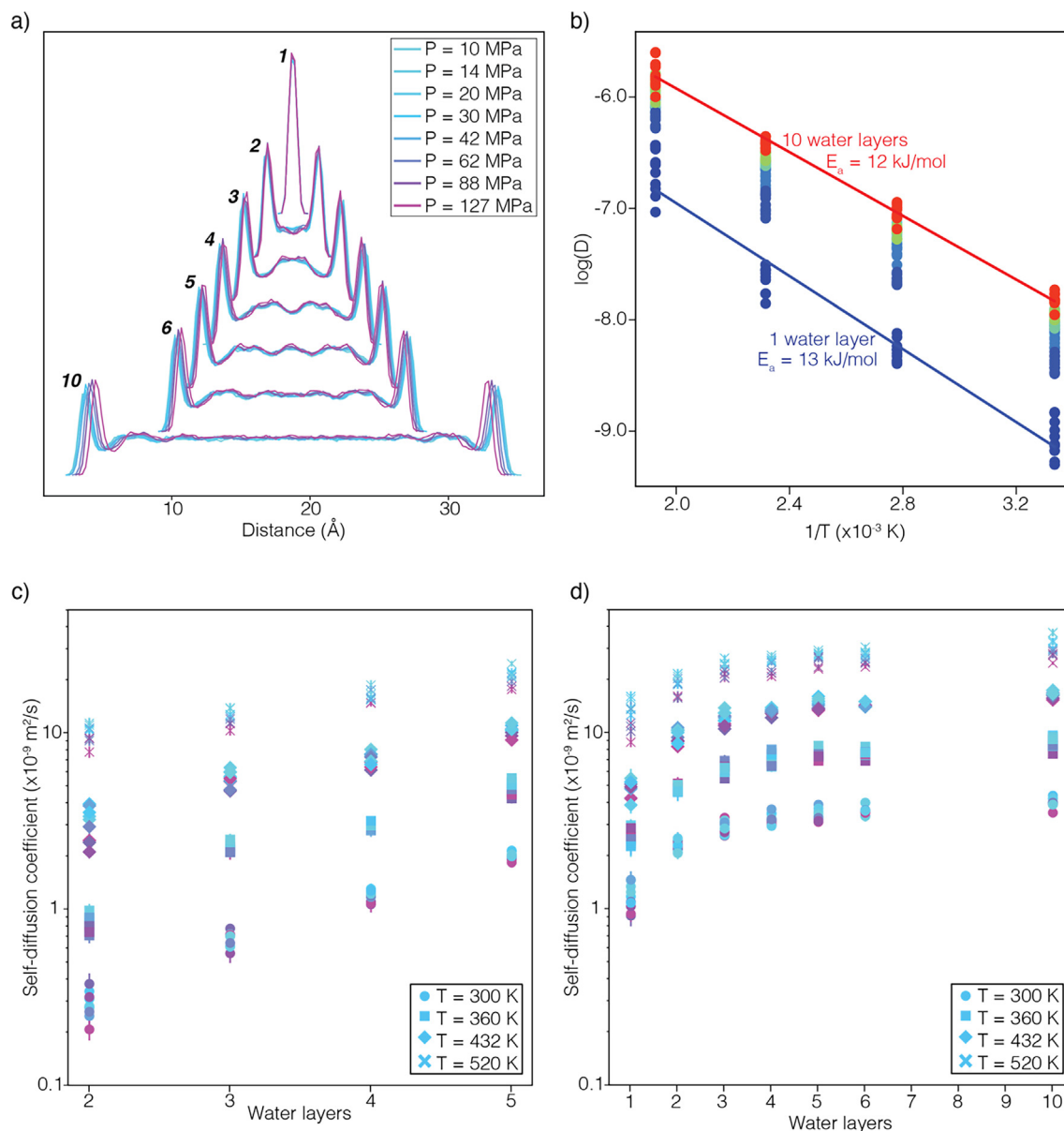


Fig. 4. Atomic density profiles and diffusion coefficient of water films confined between periclase or brucite surfaces (see Fig. 2 for geometry). (a) Atomic density profiles for the oxygen atoms in a water film confined between two brucite grains. The curves are shifted vertically for clarity. Fig. A5 displays similar profiles for the hydrogen atoms. (b) Self-diffusion coefficient of water as a function of $1/T$ for 1 (dark blue) to 10 (red) water layers between brucite surfaces. E_a = Activation energy. Fig. A6 displays a similar plot for periclase. (c-d) Self-diffusion coefficient in the xy -directions of water molecules between (c) brucite and (d) periclase slabs, calculated with mean square displacement. Each point corresponds to a pressure between 10 and 100 MPa, and is colored from low (light blue, 10 MPa) to high (purple, 100 MPa) pressure. Symbols show results at different temperatures in the range 300–520 K. (For interpretation of the references to colour in this figure legend, the reader is referred to the web version of this article.)

the plane of the water film between brucite surfaces demonstrate a structural organization of the atoms. This organization in layers with different densities is present for thin film thicknesses of up to five water layers. When the water film is thicker, only the two layers closest to each surface show a density structural organization.

The self-diffusion of bulk water, measured in the xy -directions, does not vary much with mineral interface (per-

iclase or brucite) or the pressure, with variations less than a factor of 2 in the pressure range 10–100 MPa. The temperature and water film thickness have significant effects on the self-diffusion coefficient of water molecules (Fig. 4c and d).

For periclase, the self-diffusion coefficient of water increases by a factor of 8 when the water film thickness increases from two to five water layers, and a factor of 16 when increasing the temperature from 300 to 520 K. For

brucite, the self-diffusion coefficient increases by a factor of 10 with increasing temperature in the range 300–520 K and by a factor of 3 when the film thickness increases from one to ten water layers.

The activation energy for water molecules diffusion between brucite grains (Fig. 4b) increases from 11.9 kJ/mol to 13.6 kJ/mol when the thickness of the water film decreases from ten to one water layer. For water molecules between periclase grains, the activation energy of diffusion increases from 13.9 kJ/mol to 20.9 kJ/mol (Fig. A6) when the water film thickness decreases from five to two water layers.

3.2. Behavior of a confined water film when squeezed out of grain contact

In the *Brucite-squeeze* and *Periclase-squeeze* systems, the thickness of the simulation domain (L_z , Fig. 3a) changes with time for different pressures, temperatures and slab sizes. The removal rate of water from the interface increases both with increasing pressure and with increasing temperature.

For the *Brucite-squeeze* simulations, Fig. 5a shows that with pressures in the range 40–100 MPa and temperatures in the range 432–519 K, the duration required to reach a water film thickness of one water layer is less than 1 ns while at lower pressures and temperatures this duration can increase to more than 3 ns. At a temperature of 300 K, a pressure higher than 67 MPa is required to decrease the water film thickness to one water layer, while for a temperature of 519 K, the pressure must exceed 18 MPa to reach one water layer within 2 ns.

To study the effect of the size of the brucite slab on the film thickness, we performed simulations with brucite slab sizes in the range $10\text{--}40 \times 10\text{--}40 \times 7$ unit cells repetitions. These simulations show that when the size of the brucite slab increases from 10 to 40 unit cell repetitions in the y -direction, the time required to reach a thickness of one water layer increases from less than 1 ns to more than 3 ns. Conversely, since the slab is periodic in the x -direction, we observe that increasing the size in the x -direction from $10 \times 10 \times 7$ to $20 \times 10 \times 7$ unit cell repetitions does not affect the duration to reach one water layer (Fig. A7).

For the *Periclase-squeeze* simulations we measure the time necessary to reach a water film thickness of two water layers. Fig. 5b shows that at a temperature of 300 K, the duration to reach a two-layer water film thickness is ~ 2 ns when the pressure in the range 53–100 MPa, while at lower pressure the water film thickness remains at three or four water layers after 3 ns. At 519 K, the duration to reach two water layers is less than 2 ns for all pressures in the range 15–100 MPa. The results presented in Text A2 and Fig. A2 are consistent with the *Periclase-squeeze* simulations. Fig. A2 shows that when the pressure is below 30 MPa at 453 K, the duration to reach two water layers varies from 2 to 12 ns depending on the crystallographic orientation (Fig. A2b). However, at 453 K and with a pressure above 30 MPa, the duration to reach a two water layer thickness is less than 3 ns, whatever the crystallographic orientation.

For both *Brucite-squeeze* and *Periclase-squeeze* we measured the waiting time for squeezing out the water film at a temperature of 519 K (Fig. 3b). For brucite, we measure the time needed to reach one water layer, while for periclase, we measure the time needed to reach two water layers, because the periclase surface binds water much more strongly than brucite. We interpret these results such that there is a transition between a pressure regime where it is difficult to remove the water layers to a pressure regime where it is easy to remove the water layers. In the *Brucite-squeeze* simulations at 519 K (Fig. 6), we observe that when the pressure is below 25–30 MPa, most of the simulations do not reach the one water layer level, while for pressures above 25–30 MPa a single water layer is reached within a few ns. A few simulations within the pressure range 15–25 MPa reached a water film thickness of one water layer within 2 ns. The deviation from the trend that simulations in this pressure range do not reach one water layer could be due to fluctuations pushing the system over the energy barrier to squeezing out the water film. Results from simulations with an initial shorter distance (decreased from 32 Å to 17 Å) are in agreement and indicate a transition around 25–35 MPa (Fig. A8a). In the *Periclase-squeeze* simulations (Fig. A8b), the transition between simulations that reach two water layers or not is ~ 15 MPa.

4. DISCUSSION

4.1. Water film thickness and self-diffusion coefficient of a confined water film

The water film thickness is calculated as a function of time under different pressures and temperatures. We observe that the number of water layers that can be removed from the confined water film depends on the mineral interface above and below that water film. For example, for un-hydroxylated periclase surfaces, the last two layers of water remain trapped, while for brucite only one water layer remains (Fig. 5). These results are in agreement with previous numerical and experimental studies performed on un-hydroxylated periclase, which have shown that water binds strongly to the periclase surfaces due to high surface charges and the lattice parameters that maximize interactions between water molecules and MgO units with a ratio of one water molecule for one MgO unit (Stirniman et al., 1996; Engkvist and Stone, 1999). Calculated adsorption energy of water molecules to periclase (0 0 1) and brucite surfaces support that water binds more strongly to periclase than brucite. Asaduzzaman (2020) found the adsorption energy of water molecules in a monolayer to an un-hydroxylated periclase (0 0 1) surface to be -54.5 kJ/mol. For brucite, the adsorption energy of water molecules to the brucite surface is estimated to be ~ 25 kJ/mol (Sakuma et al., 2004).

The self-diffusion coefficient of water molecules is higher between brucite surfaces than periclase surfaces. The self-diffusion coefficient is also higher in thick water films than in thin ones. The activation energy for self-diffusion increases with a decreasing water film thickness and the sensitivity of this activation energy due to water film thickness

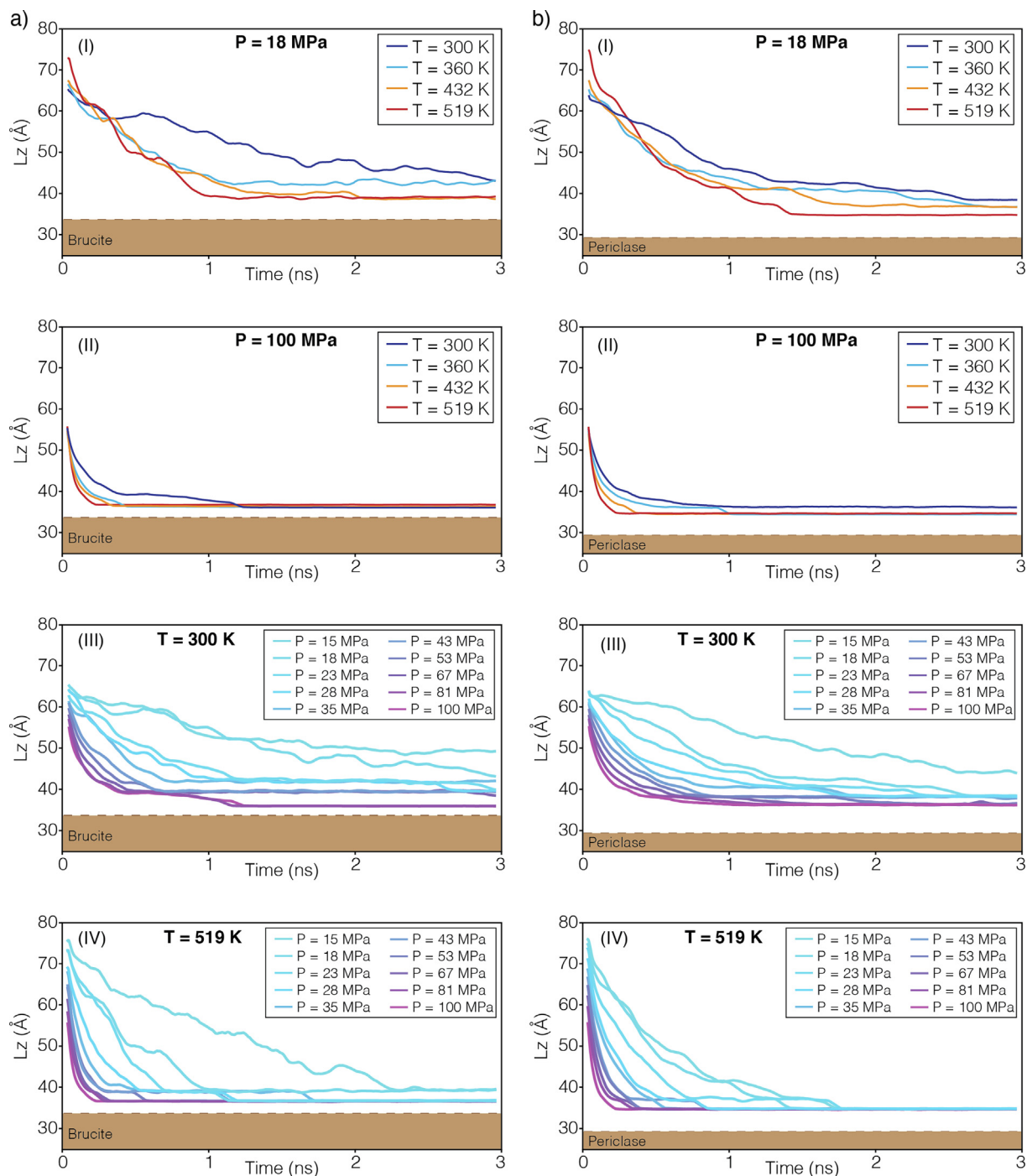


Fig. 5. Thickness (L_z) of the simulation domain in the z -direction as a function of time in the (a) *Brucite-squeeze* and (b) *Periclase-squeeze* simulations (see Fig. 3a for the geometry). (I) and (II) Simulations of the evolution of the water film thickness as a function of time for different temperatures in the range 300–519 K at two pressures (18 and 100 MPa). (III) and (IV) Simulations of the evolution of the water film thickness as a function of four different pressures in the range 15–100 MPa at two temperatures (300 and 519 K).

is higher between periclase surfaces than between brucite surfaces. Numerical studies indicate that the self-diffusion coefficient for bulk water, using single point charge water model at 300 K, is in the range $3\text{--}4 \times 10^{-9} \text{ m}^2/\text{s}$ (Yu and van Gunsteren, 2004; Guevara-Carrion et al., 2011; Tsimpanogiannis et al., 2019), while experimental studies that used nuclear magnetic resonance (e.g. Holz et al.,

2000) or a diaphragm cell (Mills, 1973; Eastale et al., 1989) report the self-diffusion coefficient of water to be $\sim 2.3 \times 10^{-9} \text{ m}^2/\text{s}$ at 300 K. These studies also report the activation energy for water molecules. From experimental studies, the activation energy is reported to be in the range 14.3–18.0 kJ/mol (Mills, 1973; Eastale et al., 1989) while numerical models report slightly lower activation energies

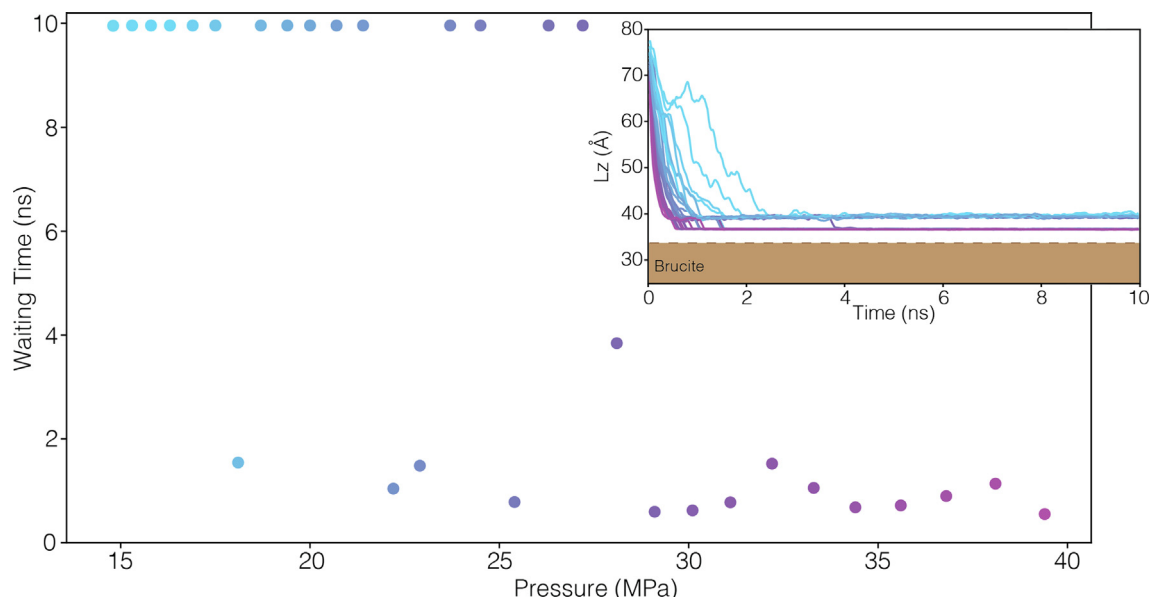


Fig. 6. Waiting time to reach one water layer for the *Brucite-squeeze* simulations. When the waiting time is equal to 10 ns, the water film thickness after 10 ns contained at least two water layers and the waiting time to reach one water layer will be longer than 10 ns. The simulations were performed in the pressure range 15–40 MPa at 519 K. The inset shows how the thickness (L_z) of the simulation domain change as a function of time during 10 ns. Each point corresponds to the waiting time for one line in the inset figure at a pressure between 15–40 MPa and both the lines and points are colored from light blue (15 MPa) to purple (40 MPa). (For interpretation of the references to colour in this figure legend, the reader is referred to the web version of this article.)

between 9.998 and 12.890 kJ/mol (Espinosa et al., 2014; Ding et al., 2016; Tsimpanogiannis et al., 2019). The latter values fit with our estimated activation energies. For a film thickness of five water layers at 300 K, the self-diffusion coefficients for water molecules between periclase and brucite interfaces are $\sim 2 \times 10^{-9}$ m²/s and $\sim 3 \times 10^{-9}$ m²/s, respectively. These diffusion rates are slightly lower than the bulk coefficients. The most likely cause is that two of the water layers bind to the surface, as indicated by e.g. Engkvist and Stone (1999) and Lee et al. (2003), decreasing the overall diffusion rate. The activation energy increases by 13 % when the water film thickness decreases from ten to one water layers between brucite surfaces and by 33 % with a reduction from five to two water layer between periclase surfaces. This indicates that the binding of water is stronger between the periclase surfaces than between the brucite surfaces, which also affects the kinetics of diffusion, even though both are hydrophilic minerals.

Several studies characterized the behavior of water on hydrophilic mineral surfaces, such as periclase and brucite (e.g. Lee and Rosky 1994; Marmier et al., 1998; Malani et al., 2009; Phan et al., 2012; Ou et al., 2014 and references therein). These studies showed that in most cases the water molecules form hydrogen bonds at the mineral surface and become structurally ordered, with a reduction in diffusion rate by a factor of 2–5 compared to bulk water. For the periclase system, the diffusion rate can be five times lower than in bulk water (Marmier et al., 1998). However, simulations performed on the brucite system indicate that, in contrast to most hydrophilic minerals, brucite barely affects the diffusion dynamic of water in a thin layer near the mineral surface (Ou et al., 2014). These results are in agreement with

our results where the diffusion coefficient of water between brucite surfaces decreases by a factor of 3 when the film thickness decreases from five to one water layers. Conversely, between periclase surfaces, the diffusion coefficient decreases by a factor of almost ten when the water film thickness decreases from five to two water layers, giving a lower self-diffusion coefficient of water molecules than between brucite surfaces. Moreover, the self-diffusion coefficient of water between brucite surfaces is also reduced substantially when the water film thickness is decreased.

4.2. Hydration forces between mineral interfaces

Several types of hydration forces operate between mineral surfaces in aqueous solutions: strongly monotonically repulsive forces, attractive forces, oscillatory forces and combinations of all three forces (e.g. Israelachvili, 2011). The existence of monotonically repulsive forces was first proposed by Langmuir (1938), and described in several other studies (e.g. Parsegian and Zemb, 2011; Kilpatrick et al., 2013; Shen et al., 2018). These studies have demonstrated the existence of two kinds of repulsive hydration forces acting over short distances, depending on the nature of the surfaces. In our case, we consider repulsive hydration forces between solid hydrophilic minerals. If the repulsive forces are smaller than the applied pressure on the system, the water film may collapse to one or two water layers, which reduces the transport properties along the grain boundaries (e.g. Weyl, 1959; Renard and Ortoleva, 1997). Our simulations show that a water film between brucite surfaces is reduced to one layer of molecules when the applied pressure exceeds 25–30 MPa. Our simulations were performed

in the pressure range 10–100 MPa. Even at 100 MPa, the remaining single water layer between the surfaces appears to be stable. Other numerical studies of solvation layers between surfaces of other minerals, such as calcite or aragonite, indicate that two or three water layers remain stable up to 1 GPa (Brekke-Svaland and Bresme, 2018).

4.3. Implications for reaction-induced fracturing

Hydration of periclase to form brucite and associated reaction-induced fracturing due to the expansion of solid volume, requires sustained supply of water to the reactive interfaces. The same applies to the hydration of peridotite to form serpentine. Previous studies of the brucite-

forming reaction show that the access of water at the reacting surface could be rate limiting. At high pressures, either the diffusion of ions is significantly slower (Kuleci et al., 2016) or the water film is squeezed out of the grain-grain contact (Zheng et al., 2018) or.

Zheng et al. (2018) quantified the periclase to brucite transition by *in situ* X-ray tomography imaging and characterized the evolution of porosity during the reaction progress. They observed two different behaviors, depending on whether the effective mean stress applied to the samples was above or below 30 MPa. In the experiments where the effective mean stress was below 30 MPa, reaction-induced fracturing was observed. The reaction proceeded through three different stages (Fig. 7a). Stage 1 was characterized by slow replacement of periclase to brucite. During stage

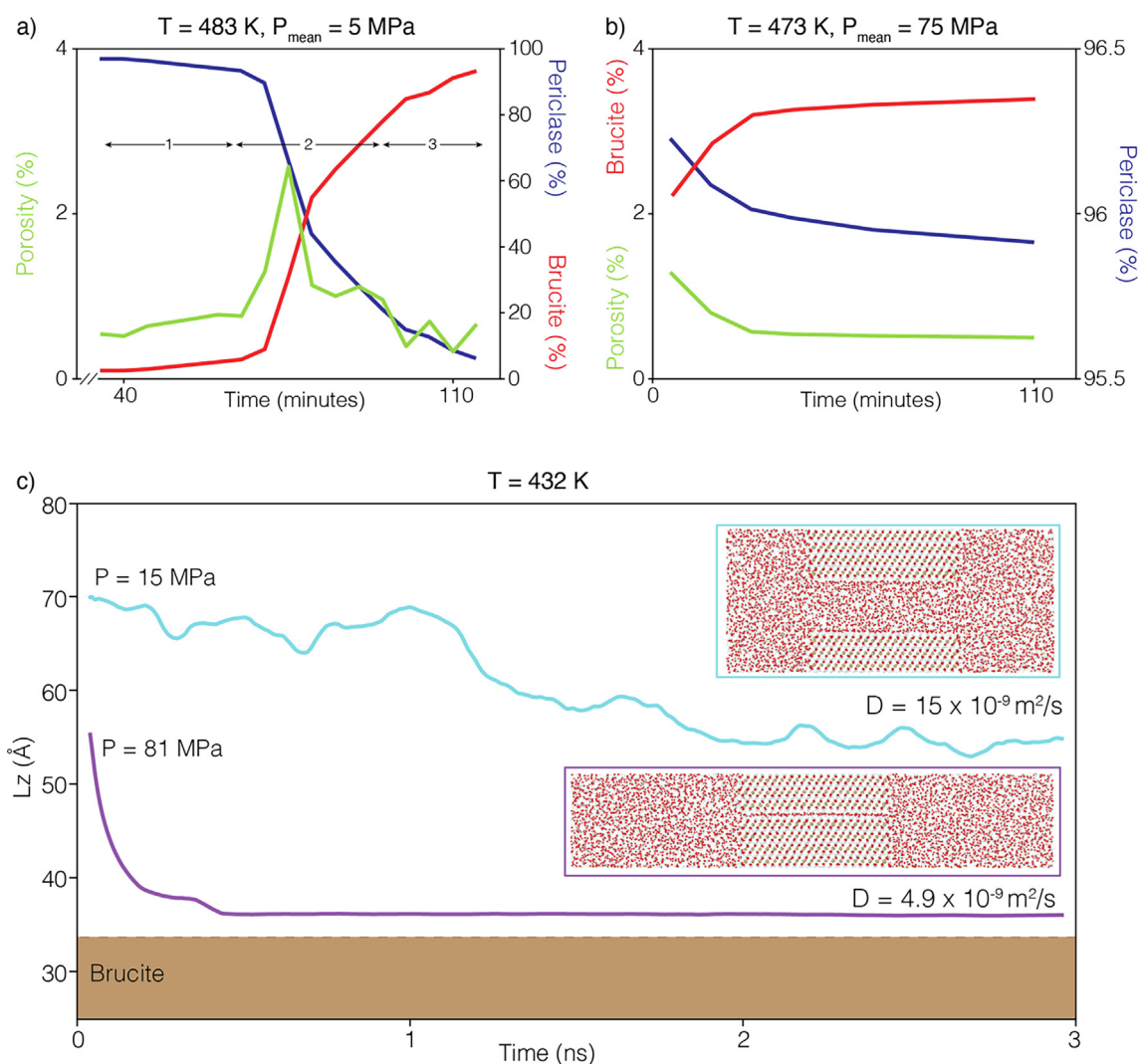


Fig. 7. (a) Evolution of porosity (green), periclase content (blue) and brucite content (red) at a temperature of 483 K and an effective mean stress of 5 MPa during the periclase to brucite reaction (modified from Zheng et al., 2018). The three stages of reaction progress and reaction-induced fracturing are indicated (1: onset of reaction, 2: fracturing induced porosity pulse and 3: pore collapse until complete reaction). (b) Evolution at a temperature of 473 K and an effective mean stress of 75 MPa. No reaction-induced fracturing occurred during the experiment (modified from Zheng et al., 2018). (c) Thickness (Lz) of the simulation domain in the z-direction as a function of time at temperature 432 K with pressures of 15 and 81 MPa. D is the self-diffusion coefficient of the water molecules in water films with the thickness at 3 ns. The inset figures are snapshots at 3 ns, visualizing the water film thickness between the two brucite blocks. (For interpretation of the references to colour in this figure legend, the reader is referred to the web version of this article.)

2, the rate of replacement increased due to the onset of reaction-driven fracturing and a pulse-like porosity increase was observed (Zheng et al., 2018). The example in Fig. 7a shows that a maximum porosity of $\sim 2.5\%$ was reached before the pore space collapsed to less than 1%. When the porosity decreases to 1% or less, the fluid transport must occur along the grain boundaries. Even though some void space along triple junctions exists in natural systems, our 3D simulations of water confined between two parallel plates is relevant to water confined along grain boundaries because in low porosity rocks, the behavior of the confined water films is the determining factor for whether water supply is shut off such that the periclase to brucite reaction stops. During stage 3, the reaction rate decreased until the replacement was complete. After 110 min (Fig. 7a), 95% of the periclase was replaced by brucite.

In contrast, for experiments carried out at mean stress above 30 MPa, reaction-induced fracturing was not observed. During the reaction, the porosity decreased from the initial 1.3% to 0.5% (Fig. 7b), and at the same time, the brucite volume increased to $\sim 3\%$, suggesting that the initial pores were clogged with brucite without producing new fractures (Zheng et al., 2018).

Fig. 7a and b show the behavior of experiments performed at 473–483 K and 5 MPa and 75 MPa, respectively. Our molecular dynamics simulations performed under similar conditions, 432 K and 15 MPa and 81 MPa (Fig. 7c) show that when the pressure is 15 MPa, below the 30 MPa limit observed in the experiments by Zheng et al. (2018), the water film thickness between two brucite surfaces consists of six water layers after 3 ns, and the self-diffusion coefficient of the water molecules is $15 \times 10^{-9} \text{ m}^2/\text{s}$. However, at 81 MPa, the water film thickness is decreased to one water layer thickness within 0.5 ns, and the self-diffusion coefficient of water molecules is reduced to $4.9 \times 10^{-9} \text{ m}^2/\text{s}$. The observed occurrence of higher porosity in the experiments below the 30 MPa limit is consistent with our simulations (Fig. 6) and indicate the reaction and fracturing can be maintained in the system when the applied pressure is reduced. However, when the pressure in the experiment is increased to 75 MPa, the reaction slows down and no fracturing occurred. Similarly, the simulation at 81 MPa shows that the water film rapidly collapses to one water layer, and the access of water to the reacting surface and ion-transportation is therefore limited.

To maintain the ion-transport along grain boundaries, the water film has to be thick enough to accommodate the hydration shell of Mg^{2+} . As periclase dissolves, the Mg^{2+} ions hydrate, and the water hydration layers are strongly bonded to the Mg^{2+} (e.g. Bo et al., 2017). Several studies have shown that the first hydration shell around Mg^{2+} ions contains six water molecules, creating a stable octahedral structure, and the second hydration shell contains twelve water molecules which are connected to the first hydration shell with hydrogen bonds (Bol et al., 1970; Pavlov et al., 1998; Bo et al., 2017). The average bond length between Mg^{2+} -water and water-water is 2.07 Å (Pavlov et al., 1998), and the distance for the second hydration shell is reported to be about 4.2 Å from the Mg^{2+} -ion (Bol et al., 1970). This implies that when the water film

thickness is reduced to one or two water layers ($\sim 3\text{--}6 \text{ \AA}$), the transfer of Mg^{2+} -ions would be limited due to space restrictions, therefore slowing down the kinetics of reaction-induced fracturing.

5. CONCLUSION

- We propose that reaction-induced fracturing requires a stable water film to proceed during the formation of brucite from hydration of periclase, and our simulations show that the pressure where the water film remains stable is below a few tens of MPa.
- When the pressure reaches a few tens of MPa, the water film between grains collapses, a process which reduces the water film thickness and the self-diffusion coefficient of water molecules. The thickness of this water film is smaller than the hydration shell around Mg^{2+} -ions which will limit ion-transportation.
- The observed slowdown in reaction-induced fracturing in the periclase-brucite system above 30 MPa effective pressure can be explained by an insufficient hydration force. When the effective pressure increases to a few tens of MPa, the access to water inside the grain contact decreases and a thin water film layer limits ion-transfer to the reacting surface.
- Our results propose that the rate of reaction-induced fracturing could be limited by the access of water to the grain boundaries, limiting the chemical reaction there. This result provides an explanation of the slowdown of reaction-induced fracturing rate observed in experimental studies of the hydration of calcium and magnesium oxides.

Declaration of Competing Interest

The authors declare that they have no known competing financial interests or personal relationships that could have appeared to influence the work reported in this paper.

ACKNOWLEDGEMENT

B.J. received support from the European Union's Horizon 2020 Research and Innovation Programm under the ERC Advanced Grant Agreement no. 669972, 'Disequilibrium Metamorphism' ('DIME'). Some of the simulations were performed using computer resources provided by UNINETT Sigma2 - The National Infrastructure for High Performance Computing and Data Storage in Norway, project number NN9272K. We thank the Associate Editor Lawrence M. Anovitz and the three anonymous reviewers for their constructive reviews that improved our manuscript.

RESEARCH DATA

Research data associated with this article can be accessed from Zenodo at <https://doi.org/10.5281/zenodo.3931763>.

APPENDIX A. SUPPLEMENTARY MATERIAL

Supplementary data to this article can be found online at <https://doi.org/10.1016/j.gca.2020.11.016>.

REFERENCES

- Allen M. P. and Tildesley D. J. (1987) *Computer Simulation of Liquids*. Oxford Science Publications.
- Asaduzzaman A. (2020) The hydration of periclase: atomistic insights from quantum-chemical look. *Chem. Phys.* **532**. <https://doi.org/10.1016/j.chemphys.2020.110694> 110694.
- Becker G. F. and Day A. L. (1916) Note on the linear force of growing crystals. *J. Geol.* **24**, 313–333. <https://doi.org/10.1017/CBO9781107415324.004>.
- Berendsen H. J. C., Grigera J. R. and Straatsma T. P. (1987) The missing term in effective pair potentials. *J. Phys. Chem.* **91**, 6269–6271. <https://doi.org/10.1021/j100308a038>.
- Bo J., Zhang Yife and Zhang Y (2017) Mechanism, kinetic model and hydrogen ion apparent diffusion coefficient in magnesium hydroxide dissolution by pressurized carbonated water. *React. Kinet. Mech. Catal.* **122**, 819–838. <https://doi.org/10.1007/s11144-017-1230-y>.
- Bol W., Gerrits G. J. A. and van Panthaleon Eck C. L. (1970) The hydration of divalent cations in aqueous solution. An X-ray investigation with isomorphous replacement. *J. Appl. Crystallogr.* **3**, 486–492. <https://doi.org/10.1107/s0021889870006738>.
- Brekke-Svaland G. and Bresme F. (2018) Interactions between hydrated calcium carbonate surfaces at nanoconfinement conditions. *J. Phys. Chem. C* **122**, 7321–7330. <https://doi.org/10.1021/acs.jpcc.8b01557>.
- Catti M., Ferraris G., Hull S. and Pavese A. (1995) Static compression and H disorder in brucite, Mg(OH)₂, to 11 GPa: a powder neutron diffraction study. *Phys. Chem. Miner.* **22**(3), 200–206. <https://doi.org/10.1007/BF00202300>.
- Cygan R. T., Liang J.-J. and Kalinichev A. G. (2004) Molecular models of hydroxide, oxyhydroxide, and clay phases and the development of a general force field. *J. Phys. Chem. B* **108**, 1255–1266. <https://doi.org/10.1021/jp0363287>.
- Correns C. W. (1949) Growth and dissolution of crystals under linear pressure. *Discuss. Faraday Soc.* **5**, 267–271.
- Ding W., Palaiokostas M. and Orsi M. (2016) Stress testing the ELBA water model. *Mol. Simul.* **42**(4), 337–346. <https://doi.org/10.1080/08927022.2015.1047367>.
- Duffy T. S., Shu J., Mao H. kwan and Hemley R. J. (1995) Single-crystal X-ray diffraction of brucite to 14 GPa. *Phys. Chem. Miner.* **22**(5), 277–281. <https://doi.org/10.1007/BF00202767>.
- Dysthe D. K., Renard F., Porcheron F. and Rousseau B. (2002) Fluid in mineral interfaces – molecular simulations of structure and diffusion 13–1–13–4. *Geophys. Res. Lett.* **29**. <https://doi.org/10.1029/2001GL013208>.
- Easteal A. J., Price W. E. and Woolf L. A. (1989) Diaphragm cell for high-temperature diffusion measurements. Tracer diffusion coefficients for water to 363 K. *J. Chem. Soc. Faraday Trans. 1* **85**(5), 1091–1097. <https://doi.org/10.1039/F19898501091>.
- Engkvist O. and Stone A. J. (1999) Adsorption of water on the MgO(001) surface. *Surf. Sci.* **437**, 239–248. [https://doi.org/10.1016/S0039-6028\(99\)00730-X](https://doi.org/10.1016/S0039-6028(99)00730-X).
- Espinosa J. R., Sanz E., Valeriani C. and Vega C. (2014) Homogeneous ice nucleation evaluated for several water models. *J. Chem. Phys.* **141**(18). <https://doi.org/10.1063/1.4897524>.
- Fukui H., Ohtaka O., Suzuki T. and Funakoshi K. (2003) Thermal expansion of Mg(OH)₂ brucite under high pressure and pressure dependence of entropy. *Phys. Chem. Miner.* **30**(9), 511–516. <https://doi.org/10.1007/s00269-003-0353-z>.
- Guevara-Carrion G., Vrabec J. and Hasse H. (2011) Prediction of self-diffusion coefficient and shear velocity of water and its binary mixtures with methanol and ethanol by molecular simulations. *J. Chem. Phys.* **134**. <https://doi.org/10.1063/1.3515262>.
- Harlov D. and Austrheim H. (2012) *Metasomatism and the Chemical Transformation of Rock: The Role of Fluids in Terrestrial and Extraterrestrial Processes*. Springer Science & Business Media.
- Holz M., Heil S. R. and Sacco A. (2000) Temperature-dependent self-diffusion coefficients of water and six selected molecular liquids for calibration in accurate 1H NMR PFG measurements. *Phys. Chem. Chem. Phys.* **2**, 4740–4742. <https://doi.org/10.1039/b005319h>.
- Hövelmann J., Putnis C. V., Ruiz-Agudo E. and Austrheim H. (2012) Direct nanoscale observations of CO₂ sequestration during brucite [Mg(OH)₂] dissolution. *Environ. Sci. Technol.* **46**, 5253–5260. <https://doi.org/10.1021/es300403n>.
- Israelachvili J. N. (2011) *Intermolecular and Surface Forces*, third ed. Academic Press, Amsterdam.
- Iyer K., Jamtveit B., Mathiesen J., Malthe-Sørenssen A. and Feder J. (2008) Reaction-assisted hierarchical fracturing during serpentinization. *Earth Planet. Sci. Lett.* **267**(3–4), 503–516. <https://doi.org/10.1016/j.epsl.2007.11.060>.
- Jamtveit B., Putnis C. V. and Malthe-Sørenssen A. (2009) Reaction induced fracturing during replacement processes. *Contrib. Mineral. Petrol.* **157**, 127–133. <https://doi.org/10.1007/s00410-008-0324-y>.
- Jamtveit B. and Hammer Ø. (2012) Sculpting of rocks by reactive fluids. *Geochem. Perspect.* **1**(3), 341–491. <https://doi.org/10.7185/geochempersp.1.3>.
- Jug K., Heidberg B. and Bredow T. (2007) Cyclic cluster study on the formation of brucite from periclase and water. *J. Phys. Chem. C* **111**, 13103–13108. <https://doi.org/10.1021/jp072889c>.
- Kelemen P. B., Matter J., Streit E. E., Rudge J. F., Curry W. B. and Blusztajn J. (2011) Rates and mechanisms of mineral carbonation in peridotite: natural processes and recipes for enhanced, in situ CO₂ capture and storage. *Annu. Rev. Earth Planet. Sci.* **39**, 545–576. <https://doi.org/10.1146/annurev-earth-092010-152509>.
- Kelemen P. B. and Hirth G. (2012) Reaction-driven cracking during retrograde metamorphism: olivine hydration and carbonation. *Earth Planet. Sci. Lett.* **345**, 81–89. <https://doi.org/10.1016/j.epsl.2012.06.018>.
- Kilpatrick J. I., Loh S. H. and Jarvis S. P. (2013) Directly probing the effects of ions on hydration forces at interfaces. *J. Am. Chem. Soc.* **135**, 2628–2634. <https://doi.org/10.1021/ja310255s>.
- Kuleci H., Schmidt C., Rybacki E., Petrishcheva E. and Abart R. (2016) Hydration of periclase at 350 °C to 620 °C and 200 MPa: experimental calibration of reaction rate. *Mineral. Petrol.* **110**, 1–10. <https://doi.org/10.1007/s00710-015-0414-2>.
- Langmuir I. (1938) The role of attractive and repulsive forces in the formation of tactoids, thixotropic gels, protein crystals and coacervates. *J. Chem. Phys.* **6**, 873–896. <https://doi.org/10.1063/1.1750183>.
- Larsen A. H., Mortensen J. J., Blomqvist J., Castelli I. E., Christensen R., Duřak M., Friis J., Groves M. N., Hammer B., Hargus C., Hermes E. D., Jennings P. C., Jensen P. B., Kermodé J., Kitchin J. R., Kolsbjerg E. L., Kubal J., Kaasbjerg K., Lysgaard S., Maronsson J. B., Maxson T., Olsen T., Pastewka L., Peterson A., Rostgaard C., Schiøtz J., Schütt O., Strange M., Thygesen K. S., Vegge T., Vilhelmsen L., Walter M., Zeng Z. and Jacobsen K. W. (2017) The atomic simulation environment – a Python library for working with atoms. *J.*

- Phys. Condens. Matter* **29**. <https://doi.org/10.1088/1361-648X/aa680e>.
- Lee S. H. and Rossky P. J. (1994) A comparison of the structure and dynamics of liquid water at Hydrophobic and hydrophilic surfaces – a molecular dynamics simulation study. *J. Chem. Phys.* **100**, 3334–3345. <https://doi.org/10.1063/1.466425>.
- Lee J. H., Eun J. H., Kim S. G., Park S. Y., Lee M. J. and Kim H. J. (2003) Hydration behavior of MgO single crystals and thin films. *J. Mater. Res.* **18**, 2895–2903. <https://doi.org/10.1557/JMR.2003.0404>.
- Malani A., Ayappa K. G. and Murad S. (2009) Influence of hydrophilic surface specificity on the structural properties of confined water. *J. Phys. Chem. B* **113**, 13825–13839. <https://doi.org/10.1021/jp902562v>.
- Malvoisin B., Brantut N. and Kaczmarek M. A. (2017) Control of serpentinisation rate by reaction-induced cracking. *Earth Planet. Sci. Lett.* **476**, 143–152. <https://doi.org/10.1016/j.epsl.2017.07.042>.
- Marmier A., Hoang P. N. M., Picaud S., Girardet C. and Lynden-Bell R. M. (1998) A molecular dynamics study of the structure of water layers adsorbed on MgO(100). *J. Chem. Phys.* **109**, 3245–3254. <https://doi.org/10.1063/1.476915>.
- Martin B. and Fyfe W. S. (1970) Some experimental and theoretical observations on the kinetics of hydration reactions with particular reference to serpentinization. *Chem. Geol.* **6**, 185–202. [https://doi.org/10.1016/0009-2541\(70\)90018-5](https://doi.org/10.1016/0009-2541(70)90018-5).
- Martinez M. J. and Martinez L. (2003) Packing optimization for automated generation of complex system's initial configurations for molecular dynamics and docking. *J. Comput. Chem.* **24**, 819–825.
- Mills R. (1973) Self-diffusion in normal and heavy water in the range 1–45°. *J. Phys. Chem.* **77**, 685–688. <https://doi.org/10.1021/j100624a025>.
- Nagai T., Hattori T. and Yamanaka T. (2000) Compression mechanism of brucite: an investigation by structural refinement under pressure. *Am. Mineral.* **85**(5–6), 760–764. <https://doi.org/10.2138/am-2000-5-615>.
- Ostapenko G. T. (1976) Excess pressure on the solid phase generated by hydration (according to experimental data on hydration of periclase). *Geochemistry Int.*, 120–138.
- Ou X., Li J. and Lin Z. (2014) Dynamic behavior of interfacial water on Mg(OH)₂ (001) surface: a molecular dynamics simulation work. *J. Phys. Chem. C* **118**, 29887–29895. <https://doi.org/10.1021/jp509373d>.
- Oviedo J., Calzado C. J. and Sanz J. F. (1998) Molecular dynamics simulations of the MgO (001) surface hydroxylation. *J. Chem. Phys.* **108**, 4219–4225. <https://doi.org/10.1063/1.475820>.
- Parsegian V. A. and Zemb T. (2011) Hydration forces: observations, explanations, expectations, questions. *Curr. Opin. Colloid Interface Sci.* **16**, 618–624. <https://doi.org/10.1016/j.cocis.2011.06.010>.
- Pavlov M., Siegbahn P. E. M. and Sandström M. (1998) Hydration of beryllium, magnesium, calcium, and zinc ions using density functional theory. *J. Phys. Chem. A* **102**, 219–228. <https://doi.org/10.1021/jp972072r>.
- Phan A., Ho T. A., Cole D. R. and Striolo A. (2012) Molecular structure and dynamics in thin water films at metal oxide surfaces: magnesium, aluminum, and silicon oxide surfaces. *J. Phys. Chem. C* **116**, 15962–15973. <https://doi.org/10.1021/jp300679v>.
- Plimpton S. (1995) Fast parallel algorithms for short-range molecular dynamics. *J. Comput. Phys.* **117**, 1–19. <https://doi.org/10.1006/jcph.1995.1039>.
- Plümper O., Røyne A., Magrasó A. and Jamtveit B. (2012) The interface-scale mechanism of reaction-induced fracturing during serpentinization. *Geology* **40**, 1103–1106. <https://doi.org/10.1130/G33390.1>.
- Pouvreau M., Greathouse J. A., Cygan R. T. and Kalinichev A. G. (2017) Structure of hydrated gibbsite and brucite edge surfaces: DFT results and further development of the ClayFF classical force field with metal-O-H angle bending terms. *J. Phys. Chem. C* **121**, 14757–14771. <https://doi.org/10.1021/acs.jpcc.7b05362>.
- Putnis A. (2002) Mineral replacement reactions: from macroscopic observations to microscopic mechanisms. *Mineral. Mag.* **66**, 689–708. <https://doi.org/10.1180/0026461026650056>.
- Putnis A. (2014) Why mineral interfaces matter. *Science* **343**, 1441–1442. <https://doi.org/10.1126/science.1250884>.
- Renard F. and Ortoleva P. (1997) Water films at grain-grain contacts: Debye-Hückel, osmotic model of stress, salinity, and mineralogy dependence. *Geochim. Cosmochim. Acta* **61**, 1963–1970. [https://doi.org/10.1016/S0016-7037\(97\)00036-7](https://doi.org/10.1016/S0016-7037(97)00036-7).
- Refson K., Wogelius R. A., Fraser D. G., Payne M. C., Lee M. H. and Milman V. (1995) Water chemisorption and reconstruction of the MgO surface. *Phys. Rev. B* **52**, 10823–10826. <https://doi.org/10.1103/PhysRevB.52.10823>.
- Ryckaert J. P., Ciccotti G. and Berendsen H. J. C. (1977) Numerical integration of the cartesian equations of motion of a system with constraints: molecular dynamics of n-alkanes. *J. Comput. Phys.* **23**, 327–341. [https://doi.org/10.1016/0021-9991\(77\)90098-5](https://doi.org/10.1016/0021-9991(77)90098-5).
- Røyne A., Jamtveit B., Mathiesen J. and Malthe-Sørensen A. (2008) Controls on rock weathering rates by reaction-induced hierarchical fracturing. *Earth Planet. Sci. Lett.* **275**, 364–369. <https://doi.org/10.1016/j.epsl.2008.08.035>.
- Røyne A. and Jamtveit B. (2015) Pore-scale controls on reaction-driven fracturing. *Rev. Mineral. Geochem.* **80**, 25–44. <https://doi.org/10.2138/rmg.2015.80.02>.
- Sakuma H., Tsuchiya T., Kawamura K. and Otsuki K. (2004) Local behavior of water molecules on brucite, talc, and halite surfaces: a molecular dynamics study. *Mol. Simul.* **30**(13–15), 861–871. <https://doi.org/10.1080/08927020412331299350>.
- Sasaki S., Takeuchi Y. and Fujino K. (1979) X-Ray determination of electron-density distributions in oxides, MgO, MnO, CoO, and NiO, and atomic scattering factors of their constituent atoms. *Proc. Jpn. Acad. Ser. B Phys. Biol. Sci.* **55**, 43–48. <https://doi.org/10.2183/pjab.55.43>.
- Scherer G. W. (2004) Stress from crystallization of salt. *Cem. Concr. Res.* **34**, 1613–1624. <https://doi.org/10.1016/j.cemconres.2003.12.034>.
- Shen Z., Chun J., Rosso K. M. and Mundy C. J. (2018) Surface chemistry affects the efficacy of the hydration force between Two ZnO(1010) surfaces. *J. Phys. Chem. C* **122**, 12259–12266. <https://doi.org/10.1021/acs.jpcc.8b02421>.
- Shinoda W., Shiga M. and Mikami M. (2004) Rapid estimation of elastic constants by molecular dynamics simulation under constant stress. *Phys. Rev. B – Condens. Matter Mater. Phys.* **69**(13), 16–18. <https://doi.org/10.1103/PhysRevB.69.134103>.
- Stirniman M. J., Huang C., Smith R. S., Joyce S. A. and Kay B. D. (1996) The adsorption and desorption of water on single crystal MgO(100): the role of surface defects. *J. Chem. Phys.* **105**, 1295–1298. <https://doi.org/10.1063/1.471993>.
- Tsimpanogiannis I. N., Moulton O. A., Franco L. F. M., Spera M. B. d. M., Erdős M. and Economou I. G. (2019) Self-diffusion coefficient of bulk and confined water: a critical review of classical molecular simulation studies. *Mol. Simul.* **45**, 425–453. <https://doi.org/10.1080/08927022.2018.1511903>.
- Wang J., Kalinichev A. G. and Kirkpatrick R. J. (2004) Molecular modeling of water structure in nano-pores between brucite (001) surfaces. *Geochim. Cosmochim. Acta* **68**, 3351–3365. <https://doi.org/10.1016/j.gca.2004.02.016>.

- Weyl P. K. (1959) Pressure solution and the force of crystallization: a phenomenological theory. *J. Geophys. Res.* **64**, 2001–2025. <https://doi.org/10.1029/jz064i011p02001>.
- Wogelius R. A., Refson K., Fraser D. G., Grime G. W. and Goff J. P. (1995) Periclase surface hydroxylation during dissolution. *Geochim. Cosmochim. Acta* **59**, 1875–1881. [https://doi.org/10.1016/0016-7037\(95\)00070-G](https://doi.org/10.1016/0016-7037(95)00070-G).
- Wolterbeek T. K. T., van Noort R. and Spiers C. J. (2018) Reaction-driven casing expansion: potential for wellbore leakage mitigation. *Acta Geotech.* **13**, 341–366. <https://doi.org/10.1007/s11440-017-0533-5>.
- Yu H. and van Gunsteren W. F. (2004) Charge-on-spring polarizable water model revisited: from water clusters to liquid water on ice. *J. Chem. Phys.* **121**, 9549–9564. <https://doi.org/10.1063/1.1805516>.
- Zeitler T. R., Greathouse J. A., Gale J. D. and Cygan R. T. (2014) Vibrational analysis of brucite surfaces and the development of an improved force field for molecular simulation of interfaces. *J. Phys. Chem. C* **118**, 7946–7953. <https://doi.org/10.1021/jp411092b>.
- Zhang L., Nasika C., Donzé F. V., Zheng X., Renard F. and Scholtès L. (2019) Modeling porosity evolution throughout reaction-induced fracturing in rocks with implications for serpentinization. *J. Geophys. Res. Solid Earth* **124**, 5708–5733. <https://doi.org/10.1029/2018JB016872>.
- Zheng X., Cordonnier B., Zhu W., Renard F. and Jamtveit B. (2018) Effects of confinement on reaction-induced fracturing during hydration of periclase. *Geochemistry, Geophys. Geosystems* **19**, 2661–2672. <https://doi.org/10.1029/2017GC007322>.
- Zigan F. and Rothbauer R. (1967) Neutronenbeugungsmessungen am brucit. *Neues Jahrb. für Mineral. Monatshefte*, 137–143.

Associate editor: lawrence M Anovitz